ACS OMEGA

http://pubs.acs.org/journal/acsodf

Article

Structural Insights into the Atomistic Mechanisms of Uric Acid Recognition and Translocation of Human Urate Anion Transporter 1

Ze'an Zhao, Yu Jiang, Lu Li, Yanyu Chen, Yongmei Li, Qunsheng Lan, Ting Wu, Cuiting Lin, Ying Cao, Kutty Selva Nandakumar, Pingzheng Zhou, Yuanxin Tian,* and Jianxin Pang*

Cite This: *ACS Omega* 2020, 5, 33421−33432

Read Online

ACCESS | Metrics & More | Article Recommendations | Supporting Information

ABSTRACT: *Background*: Human urate transporter 1 (hURAT1) is the most pivotal therapeutic target for treating hyperuricemia. However, the molecular interactions between uric acid and URAT1 are still unknown due to lack of structural details. *Methods*: In the present study, several methods (homology modeling, sequence alignment, docking, and mutagenesis) were used to explain the atomistic mechanisms of uric acid transport of hURAT1. *Results*: Residues W357-F365 in the TMD7 and P484-R487 in the TMD11 present in the hURAT1 have unique roles in both binding to the uric acid and causing subsequent structural changes. These residues, located in the transport tunnel, were found to be related to the structural changes, as demonstrated by the reduced V_{max} values and an unaltered expression of protein level. In addition, W357, G361, T363, F365, and R487 residues may confer high affinity for binding to uric acid. An outward-open homology model of hURAT1 revealed a crucial role for these two domains in the conformational changes of hURAT1. F241 and H245 in TMD5, and R477 and R487 in TMD11 may confer high affinity for uric acid, and as the docking analysis suggests, they may also enhance the affinity for the inhibitors. R477 relation to the structural changes was demonstrated by the V_{max} values of the mutants and the contribution of positive charge to the uric acid selectivity. *Conclusions*: W357-F365 in TMD7, P484-R487 in TMD11, and residues F241, H245, and R477 were found to be critical for the translocation and recognition of uric acid.

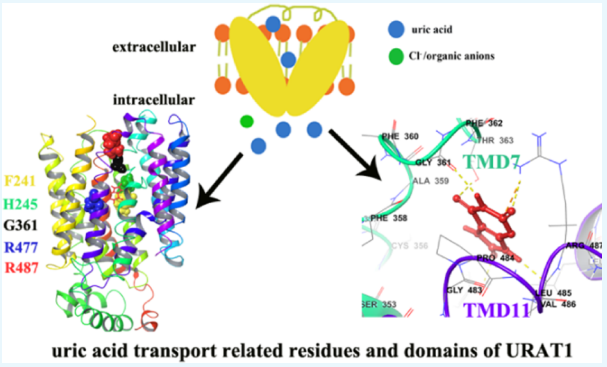

uric acid transport related residues and domains of URAT1

1. INTRODUCTION

Hyperuricemia is characterized by the presence of abnormally high level of circulating uric acid in the blood. It is mostly caused by insufficient renal excretion of urate. Many urate transporters present in the kidneys contribute to the secretion of urate, and the most important one is the hURAT1. It belongs to the organic anion transporters (OATs) subfamily[1] and the solute carrier (SLC) 22 protein family of major facilitator superfamily (MFS).[2] It plays an important role in the urate reabsorption in kidneys.[3] Many genome-wide association studies (GWAS) and targeted SNP investigations have found genetic variations in hURAT1[4−6] in patients with hyperuricemia and gout. URAT1 is expressed in the apical membrane of proximal tubule epithelial cells.[7] It exchanges urate with Cl^- and organic anions to complete the urate reabsorption. It is the most prominent transporter targeted by many widely used uricosuric agents.[4,7,8]

Members of MFS including URAT1 have a common membrane topology and similar structural characteristic MFS fold.[9] They contain two TMD hairpin structures, which are triplicated to produce six TMD units. They are further duplicated to 12 helical transmembrane domains with intracellular carboxyl and amino termini.[10] Many ingenious predictive substrate transport models like "rocker-switch"[11] and "clamp and switch"[12] were proposed for MFS transporters.[13−15] These models suggest that transporters undergo a series of conformational changes like an outward-open conformation, occluded state, and inward-open conformation to perform substrate translocation.[16] However, how the conformational changes get activated and achieved is still not clear. Although the intracellular loop between 6 and 7 of the SLC22 family was proved to be critical for the conformational change,[17] this rigid movement is considered to be insufficient to clarify the translocation processes.[18−20] So, the validation of the structural regions responsible for conformational changes is a crucial step for further understanding these changes that are occurring in the transporters. A substrate binding hinge domain in TMD11, critical for transport-related structural changes of OCT1, was identified earlier.[14]

Received: November 3, 2020
Accepted: December 8, 2020
Published: December 17, 2020

Since the crystal structures are not resolved, substrate-related residues of SLC22 transporters are yet to be fully clarified. Earlier, mutation analysis and homology modeling were used to elucidate the structure and substrate binding sites of SLC22 transporters. Though members of SLC22 family have different sequences and structural details, they do have similarity in some conserved structural features. The genomic sequence of hURAT1 is significantly similar to other organic anion transporters like OAT1, OAT3, OAT4, and OAT6,[21] and they share the same substrate, uric acid. Currently, many studies with other OATs and OCTs are being reported, including hOAT1,[22−24] hOAT4,[25] rOAT3,[26] and mOAT1[27] with their substrate binding and conformational change-related residues.[28] It should be noted that the uric acid binding pocket is formed by several TMDs.[29] So, clarifying the nature of TMDs contributing to the transport pocket and uric acid binding is an important issue. A previous report focused on inhibitor binding has identified TMD1, 7, and 11 of hURAT1 as the domains contributing to the affinity of URAT1 inhibitors. In addition, several binding sites of RDEA3170[30] with commercially available URAT1 inhibitors such as S35, F365, and I481 were identified earlier. However, how the conformational change and whole dynamic of the uric acid transport are achieved still remain unclear.

In this study, multiple approaches like homology modeling, molecular docking, sequence alignment, and mutagenesis were applied to decipher the critical residues related to uric acid transport and recognition, as well as the structural changes taking place in the hURAT1 transporter. In essence, we identified a possible outward translocation pathway for hURAT1 transporter based on two structural change-related domains and several critical residues that are recognizing the uric acid. Thus, our studies contribute new insights into hURAT1-based molecular mechanisms involved in the transport of uric acid. However, studies using inhibitors that are capable of blocking the binding of uric acid and subsequent conformational changes of hURAT1 might be more useful.

2. RESULTS

2.1. W357-F365 and G483-R487 Residues Contribute to the Structural Changes of hURAT1. Multiple sequence alignment based on earlier studies done with other SLC22 family members gave us a reference point to explore potentially critical residues involved in the uric acid transport. Since the structural details of hURAT1 are lacking, we submit the amino acid sequence of hURAT1 to CCTOP[31] to predict its topology localization of membrane spanning regions and also the orientation of segments between them (Figure S1). A previous report describing other OATs has identified many residues present in the TMD7 that conferred high affinity for substrates,[32,33] especially aromatic amino acids required for substrate occlusion after binding to the substrates.[24] Residues in TMD11 are critical for binding to the substrates and bending the helical structure.[14,34] Next, we compared the secondary structures of transporters related to handling of uric acid in the renal tubules, hOAT1 (SLC22A6) and hOAT3 (SLC22A8) by multiple sequence alignment (MSA). Here, we observed the presence of two regions of TMD7 and TMD11 with multiple conserved residues: W357, F358, F360, F362, F364, and F365 in TMD7 and G483-R487 in TMD11 (Figure 1). The conservation of these residues was predicted by consurf server, and the conscores are listed in Table S2. We

Figure 1. Representative multiple sequence alignment of urate transporters hURAT1, hOAT1, and hOAT3. The logos denote the conserved nature of each residue within the full sequence. Different residue types are shown in different colors.

proposed that these regions might also be critical for the transport of uric acid and/or structural changes.

To examine the functional role of each residue in these two regions, we constructed a PcDNA3.1(+)-hURAT1 plasmid. Alanine scanning mutagenesis for every residue, except for A359, was performed. The hURAT1 and mutants were transiently transfected into HEK293T cells. We found that the protein expression of hURAT1 was enhanced 3-fold in HEK293T-hURAT1 compared to the mock control (Figure 2A). In addition, an exact linear relationship was found between CPM values and the concentration of ^{14}C-uric acid, as tested using the liquid counter (Figure 2B). The HEK293T-hURAT1 possesses a significantly increased transport ability compared to the mock control in a dose- and time-dependent manner (Figure 2C,D). These data demonstrated the establishment and validation of ^{14}C-uric acid uptake assay system.

As a next step, using this system, uptake of 25 μM ^{14}C-uric acid by cells expressing mutants was performed. Alanine mutants, W357-F365, have dramatically reduced the transport activity (over 60%) of hURAT1. In TMD11, a significant decrease in uric acid uptake was also detected when all of the residues in the region P484-R487 (except for G483A) were mutated to alanine (Figure 3A). To clarify whether the decreased transport activities of mutants are indeed associated with the expression of membrane proteins, we isolated and quantified them by western blot. Relative membrane protein expressions of G361A and F364A in TMD7, P484A, and V486A in TMD11 (Figure 3B,C) were found to be reduced, while negligible or marginal effects were found with other mutants on the membrane expression of hUART1.

Different factors could possibly affect the contribution of mutants to the uric acid transport in mutagenesis experiments, like failure of membrane expression, poor uric acid affinity, and blunted structural changes. To explore the role of these mutant residues further in the uric acid transport, saturation kinetic analysis was conducted by measuring both the affinity and transport velocity for uric acid (10−200 μM). The K_m and V_{max} values of wild-type hURAT1 were determined to be 96 ± 18 μM and 675 ± 38 pmol/min mg, respectively (Table 11).

Significantly reduced V_{max} values were detected with G361A, F364A, P484A, and V486A mutants, which confirmed the reduction in the expression of membrane proteins. The

https://dx.doi.org/10.1021/acsomega.0c05360
ACS Omega 2020, 5, 33421−33432

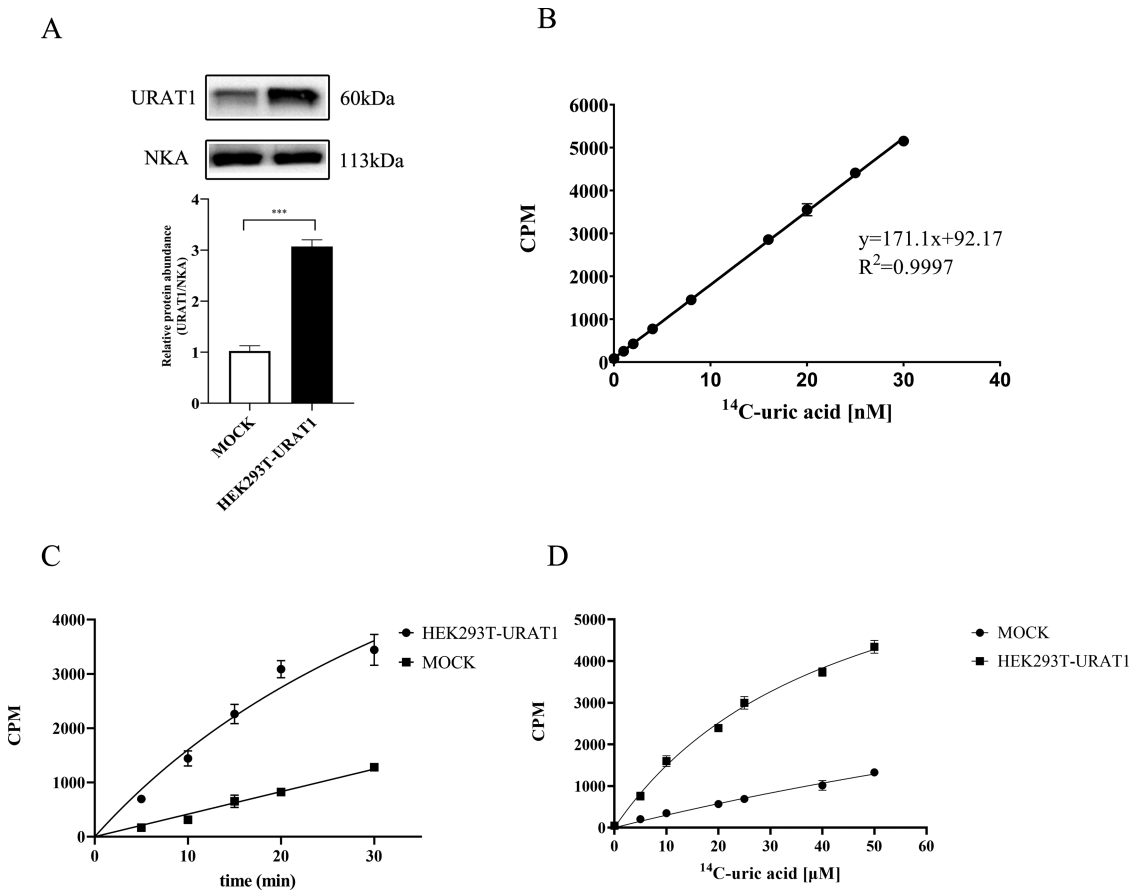

Figure 2. Construction of ^{14}C-uric acid uptake system. (A) Relative membrane protein abundance of hURAT1 and MOCK groups were determined by western blot. NKA (Na^+-K^+-ATPase) was used as an internal reference for the crude membrane proteins. (B) Standard curve of ^{14}C-uric acid (0−30 nM) was measured using a liquid scintillation counter. Time (C) and dose (D) response curves of ^{14}C-uric acid uptake in HEK293T-UTAT1 and MOCK cells. ***$p < 0.001$ vs URAT1-WT. Data are shown as mean ± SD.

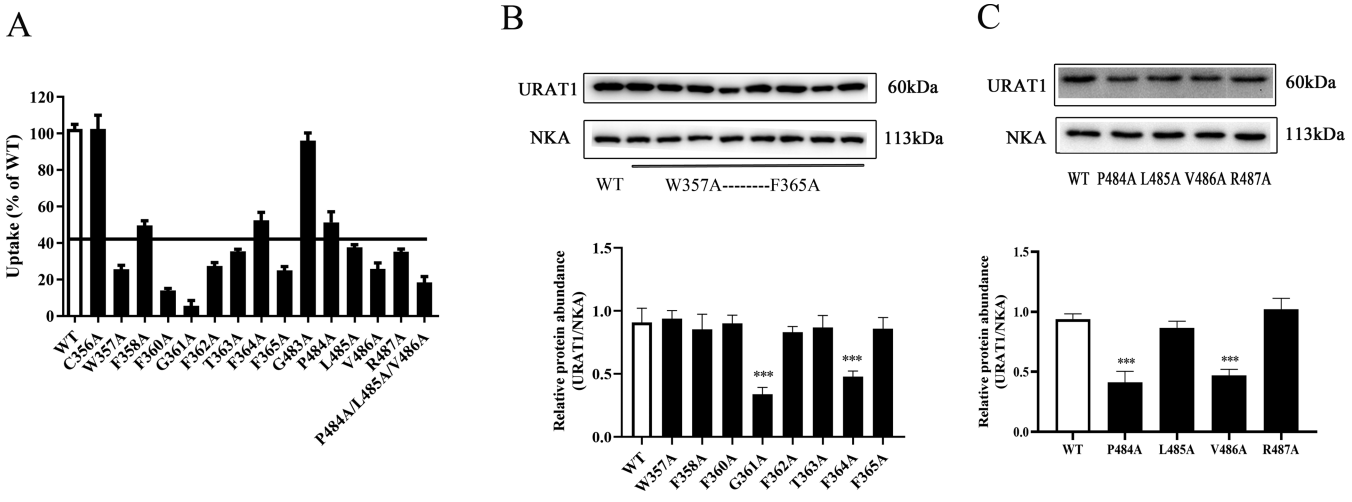

Figure 3. Effects of W357-F365 and G483-R487 mutants on uric acid transport. (A) The uric acid transport activities of proposed mutants were detected by 25 μM ^{14}C-uric acid uptake assay for 20 min in the transfected HEK293T cells ($n = 4$). (B, C) Relative membrane protein expression of hURAT1 mutants was determined by western blot. ***$p < 0.001$ vs URAT1-WT. Data are shown as mean ± SD.

reduced V_{max} values were also detected in F360A, F362A, F365A, and R487A mutants more or less, demonstrating reduction in the uric acid transport by mutation of certain specific amino acids present in hURAT1. Significantly changed K_m values were detected with W357A, G361A, F365A, and R487A mutants ($p < 0.001$), which suggests the possibility of these residues contributing to increased affinity for uric acid.

2.2. G361 and F364 Residues Are Critical for Structural Changes Related to Uric Acid Transport. In the above alanine scanning experiment, we observed that G361, F364, P484, and V486 mutants have significantly lost

https://dx.doi.org/10.1021/acsomega.0c05360
ACS Omega 2020, 5, 33421−33432

Table 1. Kinetic Analysis of W357-F365 and P484-R487 Mutants[a]

mutants	K_m (μM)	V_{max} (pmol/min mg)
WT	82 ± 32	612 ± 47
W357A	152 ± 27**	559 ± 102 (ns)
F358A	144 ± 34*	497 ± 58*
F360A	132 ± 42 (ns)	424 ± 61**
G361A	228 ± 19***	247 ± 43***
F362A	121 ± 26 (ns)	457 ± 89*
T363A	151 ± 47*	389 ± 59**
F364A	77 ± 24 (ns)	314 ± 78**
F365A	187 ± 37***	421 ± 56**
P484A	144 ± 21*	529 ± 42*
L485A	64 ± 23 (ns)	358 ± 37***
V486A	124 ± 24(ns)	374 ± 36**
P484A/L485A/V486A	167 ± 23**	284 ± 29***
R487A	189 ± 36***	406 ± 45***

[a]Results shown are from saturation transport kinetic experiments measuring the affinity (K_m) and transport velocity (V_{max}) for uric acid. *p < 0.1, **p < 0.01, ***p < 0.001, vs WT (n = 4 for mutants).

their ability for uric acid transport, especially the G361 mutant. However, the reduced expression of membrane protein has limitations in verifying their capacity for structural changes. Here, we constructed another two mutants G361S and F364Y (Note: P484 and V486 mutants having a minimal effect on the expression of membrane proteins were not obtained) with reduced transport activity and having a negligible effect on the expression of membrane proteins (Figure 4A,B). We observed that the G361S mutant has almost lost 95% of transport capacity compared to the wild type (WT), while the F364Y mutant has lost 30% of its ability for uric acid transport compared to the wild type. As a next step, kinetic analysis was performed and the K_m values were found to be significantly increased (2.5-fold) when G361 was converted to a serine mutant. This result suggested contribution of G361 mutant to the structural changes of the protein and decrease in the affinity to uric acid. The changes in V_{max} values confirmed the decreased capacity for uric acid transport in the G361S mutant (Figure 4C). Hence, it is clear that G361 could have a profound influence on the movement of the transporter. The F364Y mutant showed a reduced V_{max} value for uric acid transport with an unaltered membrane expression level. In conclusion, we can say that the G361 residue participates in binding to the uric acid and its transport, whereas F364 residue, albeit its importance, is not a primary residue participating in the structural movement of hURAT1.

2.3. R477 Is Crucial for Uric Acid Selectivity and Structural Changes in hURAT1. Organic moieties are the key structural elements of transporters, and based on their structure, either they form hydrogen bonds or are involved in hydrophobic interactions, in addition to their contribution toward net charge. OATs and organic cations (OCTs) are members of the SLC22 family. OCT transporters are capable

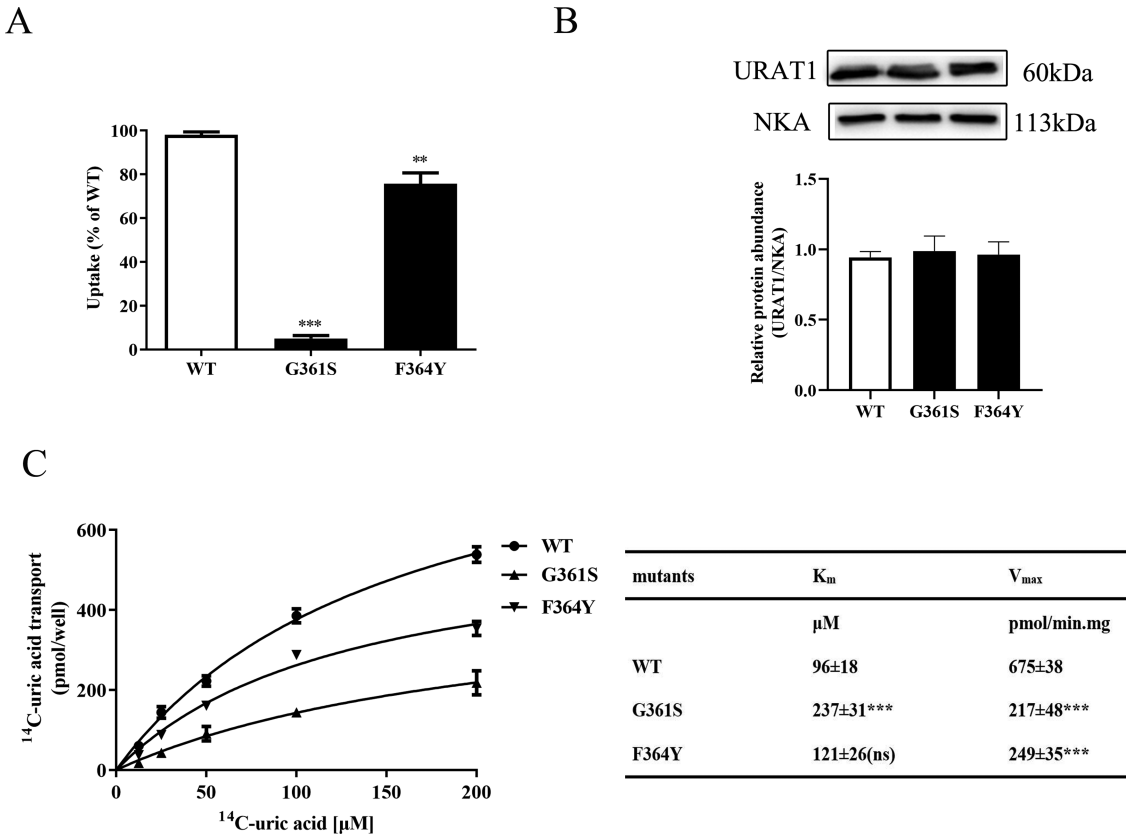

mutants	K_m	V_{max}
	μM	pmol/min.mg
WT	96±18	675±38
G361S	237±31***	217±48***
F364Y	121±26(ns)	249±35***

Figure 4. G361 and F364 residues are important for the transport-related structural changes of hURAT1. (A) ^{14}C-uric acid transport activities of G361S and F364Y mutants (n = 4/mutant). (B) Relative membrane protein abundance of G361S and F364Y mutants were determined by western blot. (C) Michaelis−Menten curves and parameters (K_m and V_{max}) of ^{14}C-uric acid kinetic measurement in HEK293T cells expressing hURAT1 and its G316S and F364Y mutants. Uric acid uptake assay was performed by incubating the transfected HEK293T cells in uptake buffer containing 10−200 μM of uric acid for 20 min. Data are shown as mean ± SD. **p < 0.01 vs WT: ***p < 0.001 vs WT.

https://dx.doi.org/10.1021/acsomega.0c05360
ACS Omega 2020, 5, 33421−33432

```
Conservation:          5 95 5   5     755599799 595575  R4776 955  96
hURAT1          439    VLGLGGVGAAFTCITIYSSELFPTVLRMTAVGLGQMAARGGAILGPLVR-   487
hOAT3           416    VFGKGCLSSSFSCLFLYTSELYPTVIRQTGMGVSNLWTRVGSMVSPLVK-   464
rOAT3           416    VFGKGCLSGSFSCLFLYTSELYPTVLRQTGMGISNVWARVGSMIAPLVK-   464
rOAT1           428    VLGKGCLASSFNCIFLYTGELYPTVIRQTGLGMGSTMARVGSIVSPLVS-   476
hOAT1           428    VLGKGCLAASFNCIFLYTGELYPTMIRQTGMGMGSTMARVGSIVSPLVS-   476
hOTA2           434    VMGKAFSEAAFTTAYLFTSELYPTVLRQTGMGLTALVGRLGGSLAPLAA-   482
rOAT2           434    VVGKAFSEAAFTTAYLFTSELYPTVLRQTGLGLTALMGRLGASLAPLAA-   482
mOCT3           435    TLGRLGITMAFEIVYLVNSELYPTTLRNFGVSLCSGLGDFGGIIAPFLLF   484
mOCT2           437    CLGRMGITIAYEMVCLVNAELYPTYIRNLAVLVCSSMGDIGGIVTPFLVY   486
hOCT2           437    CLGRMGITMAYEIVCLVNAELYPTFIRNLGVHICSSMGDIGGIITPFLVY   486
mOCT1           437    CLGRMGATIVLQMVCLVNAELYPTFIRNLGMMVCSALGDLGGIFTPFMVF   486
hOCT1           436    CVGRMGITIAIQMICLVNAELYPTFVRNLGVMVCSSLGDIGGIITPFIVF   485
Consensus_aa:          hhG+.ths.t@phlhLhstELYPThlRphGh.lts.htchGthlsPhh..
Consensus_ss:          hhhhhhhhhhhhhhhhhhhh  hhhhhhhhhhhhhhhhhhhhhhhhh
```

Figure 5. Multiple sequence alignment of OATs and OCTs. R477 is highly conserved in OATs. Residues equivalent to R477 of hURAT1 in OATs contain positively charged arginine (R), while residues in OCTs are negatively charged aspartic acid (D).

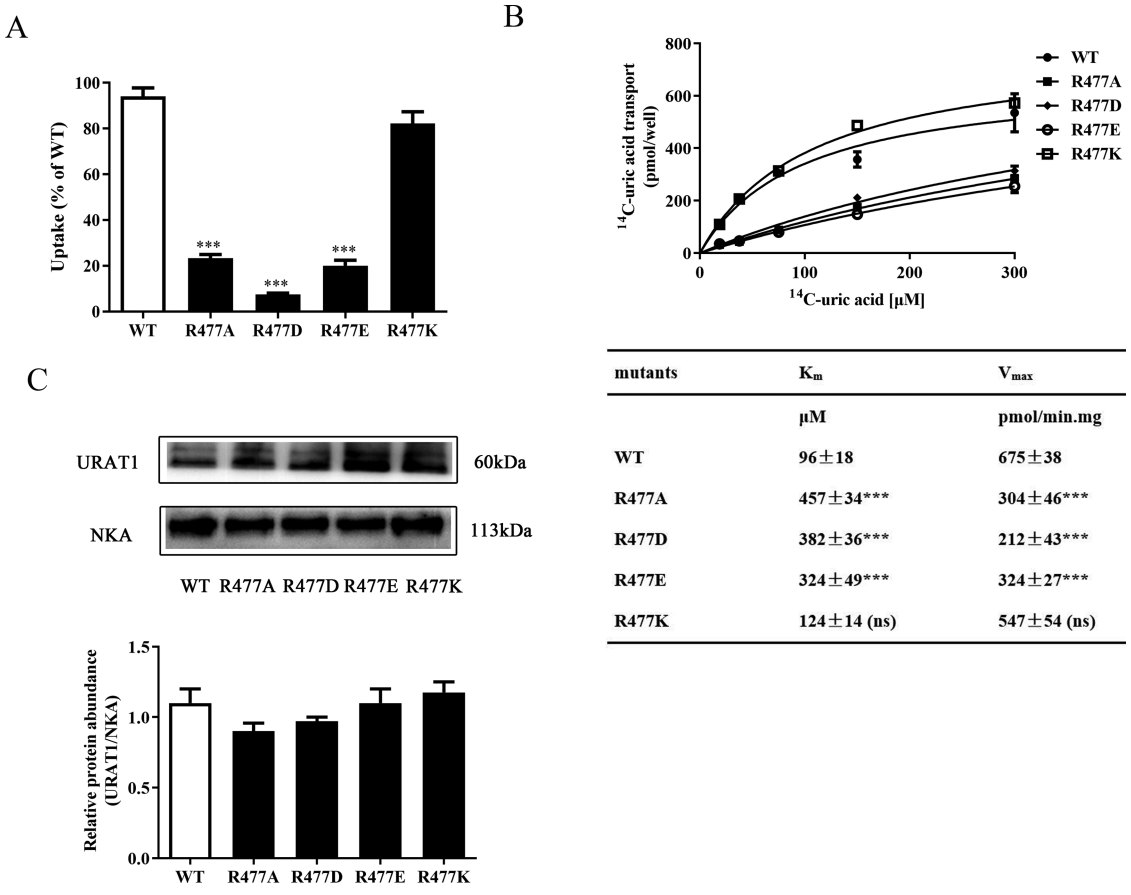

mutants	K_m	V_{max}
	μM	pmol/min.mg
WT	96±18	675±38
R477A	457±34***	304±46***
R477D	382±36***	212±43***
R477E	324±49***	324±27***
R477K	124±14 (ns)	547±54 (ns)

Figure 6. Effect of R477 mutants on the uptake of uric acid and expression of cell membrane proteins. (A) ^{14}C-uric acid transport activities of WT and R477 mutants (n = 4/mutant). (B) Kinetic study of WT hURAT1 and its mutants was performed as described in M&M section. (C) Relative membrane protein abundance of WT and hURAT1 mutants. Data are shown as mean ± SD. ***p < 0.001 vs WT. ns, not significant.

of transporting organic cations, while OATs transport the smaller and more hydrophilic organic anions. An aspartate residue in the TMD11 was identified to be conserved in all of the OCTs, but in OATs, an arginine residue is present at this position. Exchange of oppositely charged residues led to loss of function, which suggests the crucial role of charge in the binding activity to substrates.[12] Based on this observation, sequence alignment of OATs and OCTs was performed. As shown in Figure 5, R477 in hURAT1 and the corresponding residues in other OATs are all positively charged in this position.

To assess the contribution of positively charged R477 in uric acid binding, it was mutated to other charged residues, either as negatively charged residues like aspartic acid and glutamic acid or as positively charged lysine. All of the mutants were then transferred to HEK293T cells to determine ^{14}C-uric acid transport activity. We found that ^{14}C-uric acid uptake was not significantly affected when R477 was mutated to lysine. By contrast, uric acid transport was strongly reduced when R477

https://dx.doi.org/10.1021/acsomega.0c05360
ACS Omega 2020, 5, 33421−33432

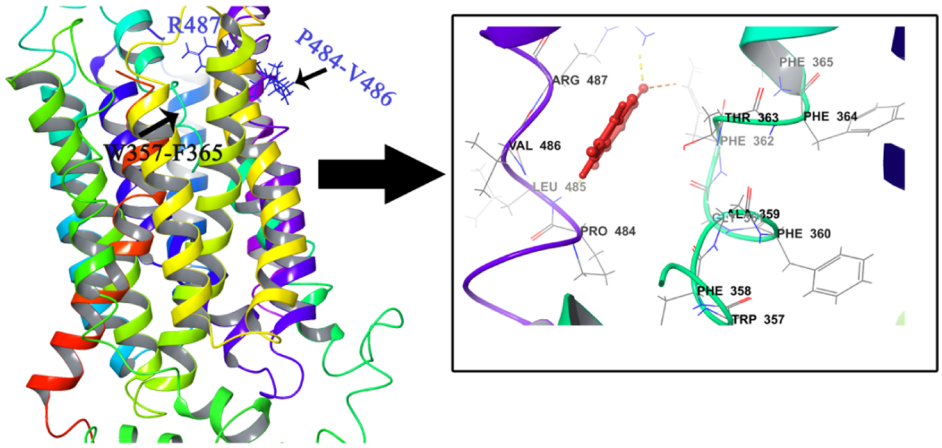

Figure 7. 3D structure of hURAT1, as generated by the homology model. The structural information of the two proposed domains and binding pocket of uric acid (red) is shown in a model of outward conformation: W357-F365 in TMD7, P484-R487 in TMD11.

was mutated to alanine, aspartic acid, or glutamic acid (Figure 6A). To determine whether the reduced transport activities were limited by the expression of membrane proteins, all of them were isolated and quantified by western blot. However, no significant reduction in the membrane proteins was detected in all of the mutants compared to hURAT1-WT (Figure 6B).

Kinetic studies revealed that all of the R477 mutants have significantly increased K_m values (3- to 4-fold) toward hURAT1, which typically increased from 96 ± 18 μM (WT) to 382 ± 36 μM (R477A), 382 ± 36 μM (R477D), and 470 ± 24 μM (R477E), respectively (Figure 6C). Increased K_m values indicated that mutants had an altered protein structure and subsequent reduction in the affinity to uric acid. However, R477K mutant displayed similar K_m and V_{max} values to wild type, suggesting the transport capacity of this mutant was unaffected. However, significantly reduced V_{max} values were detected in other R477 mutants (Figure 6C). Interestingly, the uric acid transport of hURAT1 was also reduced by mutating R477 with alanine, aspartic acid, and glutamic acid. So, R477 might play a pivotal role in both the transport-related structural movements and conferring high affinity to uric acid.

2.4. Homology Structure of Outward-Open hURAT1 Model. To have a better three-dimensional understanding of the uric acid binding and transport, we constructed a homology model in an outward-open state. Since the sequence identity was less than 30%, we first investigated the transmembrane regions of hURAT1 during *in silico* analysis by CCTOP web server (http://cctop.enzim.ttk.mta.hu). As a novel consensus topology prediction tool, it integrated 10 state-of-the-art topology prediction methods and gave much more reliable results. It predicted 12 transmembrane helices present in the protein. Then, we used I-TASSER[35] and Consurf sever to generate models for comparison. I-TASSER used advanced algorithms (multiple threading alignments) to provide precise structure prediction models (Table S3).

The top1 model from I-TASSER was in agreement with the topological structural character of SLC22 family having 12 transmembrane helices. There was a large extracellular loop in TMD1 and TMD2, and some small helical regions were present in between the TMD6 and TMD7. Combined with the knowledge of evolutionarily conserved residues based on the phylogenetic relations from ConSurf server, the multiple threading templates (PDB code: 5C65, 4J05, 4GBY, and 4GC0) were selected to generate our models. Based on various multiple alignments, 20 initial models were generated with MODELLER 9.13 software.[36] The models were ranked and evaluated by Z-DOPE score, which is a normalized atomic distance-dependent statistical potential based on known protein structures.[37] The top1 model was further minimized by Amber12. Finalized hURAT1 models were evaluated by SAVES (Structural Analysis and Verification Server) online server from UCLA (http://services.mbi.ucla.edu/SAVES/).[38] Results are listed in Figure S1. ERRAT check showed that the overall quality factor for the constructed structure of hURAT1 was 94.2, which is comparatively higher than the reported values of hOAT1 model (91.7)[24] and the crystal structure of phosphate transporter, PiPT.[39] The Ramachandran plot showed that >95% of residues were all acid residues located in the favored and allowed regions (Figure S2).

The final structure of hURAT1 displayed an outward conformation and contained 12 major helices. The cleft between TMD1-6 and TMD7-12 may be the transport channel. All of the evaluation results indicated that the final structure constructed for hURAT1 is a reasonable one and thus suitable for further investigations.

2.5. Structural Insight into Uric Acid Transport in an Outward-Open State. With the help of the homology model, we focused our effort to get an insight into uric acid transport pathway in an outward-open model. We have identified that both the W357-F365 and P484-R487 regions are related to structural changes in the uric acid transport. Consistent with this idea, we found that W357-F365 region is in fact located in the innermost part of the transport cleft between TMD1-6 and TMD7-12, whereas P484-R487 region is located in the barrier of membrane milieu, while the backbones and the side chains face the inner part of the transport tunnel (Figure 7).

Next, we performed molecular docking studies to clarify the substrate/protein interactions to support our findings in mutagenesis experiments. Since the extracellular large variable loop region between TMD1 and TMD2 (41−140 aa) and the tail of TMD12 (531−553 aa) are distal from the substrate binding site, they are most unlikely to affect the uric acid binding directly. Hence, they were omitted from the model before performing the docking experiment. Uric acid was docked to the cleft and hydrogen bonds were observed between G361, T363, and F365 (not shown) in TMD7, and V486 and R487 in TMD11 with uric acid (Figure 8A). R477

https://dx.doi.org/10.1021/acsomega.0c05360
ACS Omega 2020, 5, 33421−33432

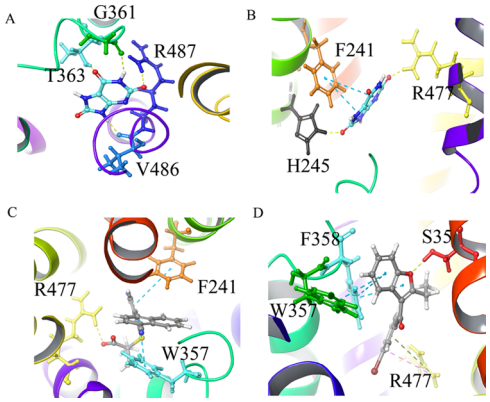

Figure 8. Interactions of uric acid and inhibitors with hURAT1. Schematic representation of possible interactions between hURAT1 and uric acid (A, B), and the inhibitors verinurad (C) and benzbromarone (D) as predicted by molecular docking studies. The positions with highest-ranking Glide scores were reported here to demonstrate the binding details.

residue is critical for selectivity of uric acid as shown above and the side chain of R477 showed possible formation of hydrogen bond with the uric acid. In addition, F241 and H245 residues located on TMD5 with the side chains facing uric acid are capable of forming possible $\pi-\pi$ stacking interactions between the aromatic rings and uric acid (Figure 8B). These docking results are consistent with our experimental results described above.

Furthermore, we investigated the importance of the identified hURAT1 residues for their interactions with the URAT1 inhibitors. We did docking experiments with the highly potent hURAT1 inhibitors verinurad (Figure 8C) and benzbromarone (Figure 8D) having the IC50 values of 0.22 and 0.025 μM, respectively. The docking results indicated that uric acid binding residues such as F241 and R477 could also interact with the inhibitors. Consistent with our results, earlier, Perry et al.[24] have constructed a Y230F mutant of hOAT1 and found its important function in the recognition of substrates, which is equivalent to F241 of hURAT1 by sequence alignment. R477 is also the binding site for verinurad as reported earlier.[30] Besides, we observed the interactions of inhibitors with the structural change-related residues like W357 and F358 in TMD7, but further experiments are needed to verify this observation.

To support our docking results, we constructed more mutants of F241, H245, and R487, substituted with the relative residues of hOAT1/3 (F241Y, H245Q, and R487K and R487S) (Figure 9A). F241A and H245A but not F241Y and H245Q mutants showed reduced ^{14}C-uric acid transport activities. In addition, the reduced transport activities of alanine mutants of F241 and H245 were found to be not due to the reduced expression levels of membrane proteins (Figure 9B). Further kinetic analysis showed increased K_m values for

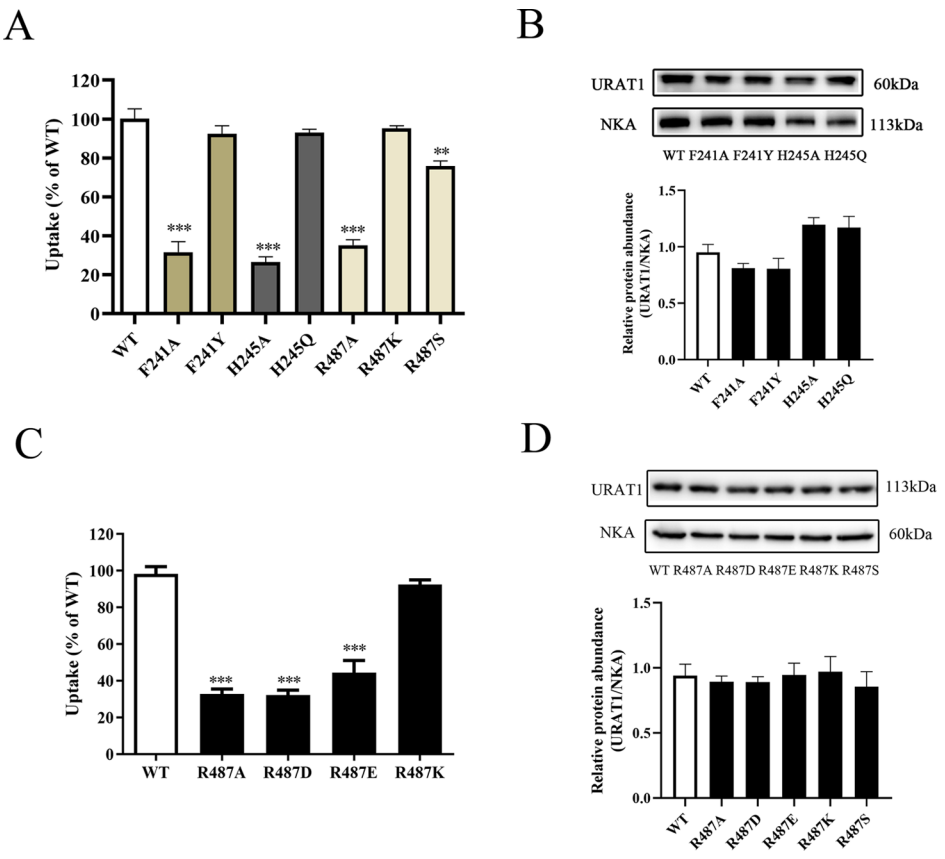

Figure 9. Identification of active sites predicted by docking analysis. (A) The uric acid uptake activities of various hRUAT1 mutants based on our docking analysis. (B) Relative expression of membrane proteins in the F241 and H245 mutants. (C) More mutants with negatively charged R487 residue of hURAT1 were examined to prove the role of positively charged R487 residue in the substrate binding activity and relative expression of membrane proteins (D). Data are shown as mean ± SD (n = 3). $^{**}p < 0.01$, $^{***}p < 0.001$ vs WT.

https://dx.doi.org/10.1021/acsomega.0c05360
ACS Omega 2020, 5, 33421−33432

F241A and H245A mutants. This result suggests that F241 and H245 residues may confer high affinity for uric acid (Table 2).

Table 2. Kinetic Analysis of F241 and H245 Mutants[a]

mutants	K_m (μM)	V_{max} (pmol/min mg)
WT	76 ± 46	601 ± 45
F241A	148 ± 32*	416 ± 44**
F241Y	74 ± 24 (ns)	634 ± 36 (ns)
H245A	164 ± 31*	651 ± 27 (ns)
H245Q	72 ± 35	647 ± 42 (ns)

[a]Saturation transport kinetic experiments measuring the affinity (K_m) and transport velocity (V_{max}) for uric acid were used. *$p < 0.1$, **$p < 0.01$, ns, not significant vs WT ($n = 6$ for WT, $n = 4$ for mutants).

Interestingly, positively charged R487K mutant showed no significant reduction in the transport activity compared to the wild type while R487S mutant showed slightly reduced transport activity ($p < 0.01$). To evaluate the contribution of the charge, R487 residue was substituted with differently charged amino acids (D and E). The mutants without having a positively charged residue at R487 lost almost 60% of their transport activity (Figure 9C) with no significant reduction in the level of membrane proteins (Figure 9D). This result suggests a critical role for the positively charged R487 residue in the translocation of uric acid. In conclusion, we provide here a visual evidence for substrate binding activity of the transport domains described above.

3. DISCUSSION

The hURAT1 is a unique therapeutic target for the reabsorption of urate in kidneys.[40] It is recognized that URAT1 inhibitors having high potency and selectivity are the future drugs for treating hyperuricemia and gout.[41] However, the mode of uric acid transport and the accompanied structural exchanges in hURAT1 are not yet clear. This calls for greater understanding of the uric acid transport through URAT1. In the big MFS family, many researchers have used homology models to aid their functional work, as in rOCT1[14] and hOAT1[24] studies. The transport mechanisms of OAT family are significantly similar to phosphate transporter, PiPT,[42,43] for which the crystal structure was resolved earlier. The conformational exchanges of PiPT are activated by binding of the substrate with an aspartic residue, which meditated alternate breaks and reformed the structure during conformational cycles. The aspartic residues[44,45] are presumed to be located in the center of the ion translocation pathway, which allowed the activation of the changes in the structural state.

Based on the homology structure of hURAT1 we generated, the proposed transport mechanism of hURAT1 seems reasonable and in accordance with the PiPT. The MFS has many common structural features; the innermost TMDs 1, 4, 7, and 10 are located in the center of the transporter, whereas TMDs 2, 5, 8, and 11 are positioned outside of the innermost TMDs. All of these TMDs are composed of a specific binding pocket for the substrates. In the model of hURAT1, the uric acid binding cleft is formed by TMD1, 5, 7, 10, and 11. Previous mutagenesis data suggested that S35 in TMD1, F365 in TMD7, and R477 and I481 in TMD11 are involved in the binding with inhibitors;[30] however, whether the uric acid interacts with these residues and/or involved in the structural changes is not yet clear.

Out study was aimed to explore the details in the conformational changes occurring in hURAT1. Two domains (TMD7 and TMD11) acting as a hinge were reported to be related with structural changes, and some of them could possibly confer high affinity for uric acid. Glycine may provide flexibility for such movements from a structure biology point of view.[46] The glycine residue G361 is located in the central part of cleft surrounded by W357 and F365 residues that are involved in the binding to uric acid. Experimental data demonstrated the importance of G361 not only in conferring high affinity to uric acid but also related to structural changes, which altered the transport kinetics. In TMD11, the P484-V486 region is conserved in urate transporters and located on the other side of the cleft. P484-V486 region cooperated with W357-F365 to accomplish the structural changes, while R487 is located on the upward side and conferred affinity for uric acid. It appears that hinge domains might be critical for substrate transport, and hence further validation is needed using other transporter systems. A similar hinge domain can also be found in rOCT1. Egenberger et al.[47] have identified a substrate binding domain in the middle of TMD11 (residues 474−478), which is conserved in OCTs and found to be critical for transport-related structural changes of organic cation transporter 1.

Currently known MFS structures were resolved to contain inward,[48,49] outward,[50] and occluded[51,52] conformations. All of the structurally elucidated MFS transporters contain a single substrate binding cavity located in the center of the membrane.[53,54] During the transport process, how the binding pocket is exposed to various residues for translocation of uric acid and its interactions with the transporter provide a strong

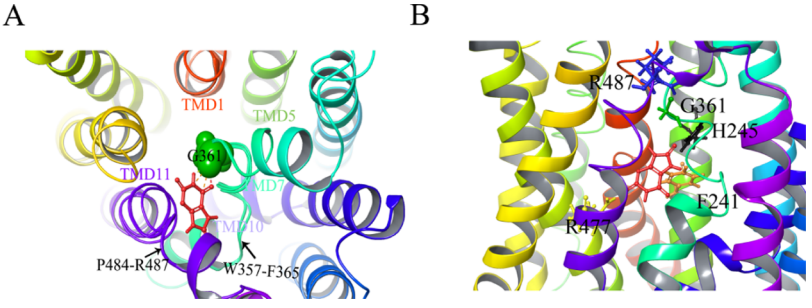

Figure 10. Proposed uric acid translocation pathway in the outward conformation of hURAT1. Two hinge domains, W357-F365 in TMD7 and P484-R487 in TMD11, and the critical residue G361 (green) are shown from the top view (A). Residues G361 (green), F241 (orange), H245 (black), R477 (yellow), and R487 (blue) were identified as important residues, which interacted with uric acid as shown in the horizontal (B) view.

https://dx.doi.org/10.1021/acsomega.0c05360
ACS Omega 2020, 5, 33421−33432

basis for designing new drug strategies. Herein, we provided new structural insights into uric acid translocation by hURAT1 (Figure 10) in an outward conformation to deliver the uric acid across the hydrophobic membrane. hURAT1 switches the conformation from the outward that facilitates uric acid binding in the extracellular side to inward conformation that can release the substrate into the intracellular side. Uric acid is transported through the tunnel composed of TMD1, 5, 7, 10, and 11. Two domains in TMD7 (W357-F365) and TMD11 (P484-R487) are proposed to be essential, which can contribute to the structural changes. Besides, some of them (W357, G361, T363, F365, and R487) could confer high affinity for uric acid.

Except for the conformational change-related domains, residues facing the binding pocket help in the uric acid translocation processes, like F241 and H245 present in the TMD5, as determined by molecular docking experiments. Sequence alignment analysis was also showing the importance of R477 in TMD11. The positive net charge of the basic amino acid is critical for the interactions with uric acid. Consistent with this study, Perry et al.[24] have shown that R466 is indeed located at the opening of the pocket affecting the transport of the substrates. Significantly reduced V_{max} value detected for R466K mutant without altering the expression of membrane protein indicated the possible contribution of R466 to the structural changes in hOAT1.[55] Another positively charged R487 residue present in the hinge domain was found to enhance the affinity to uric acid. Also, the residues we identified to be uric acid transport-related residues may contribute to the interactions with the inhibitors as well. F241 and R477 residues conferred high affinity for the URAT1 inhibitor, verinurad (RDEA3170). The IC50 value of verinurad was significantly increased when F241 and R477 residues were mutated, and the inhibitor bound to the sites by a competitive mechanism. Identifying the optimal conditions for structural modifications and designing URAT1 inhibitors seem to be an arduous task.[56] Hence, our observations could possibly give a meaningful reference for future drug designs.

4. CONCLUSIONS

In summary, our results provide an opportunity to explore the uric acid transport processes of hURAT1, which involve structural change-related domains, and substrate binding residues. W357-F365 in TMD7, P484-R487 in TMD11, and residues F241, H245, and R477 were found to be critical for translocation and recognition of uric acid. Unlike other substrate binding studies, our results explain the uric acid transport mechanisms of hURAT1 and provide critical information for designing more potential hURAT1 inhibitors focused on these residues to treat hyperuricemia and gout. It is of importance to note that inhibitors may block transport activity not only by competitive binding to the substrates but also by preventing the transport-related structural changes in an outward-open conformation.

5. MATERIALS AND METHODS

5.1. Reagents. All of the reagents were of analytical grade and purchased from Sigma-Aldrich Ltd. (St Louis, MO) unless otherwise stated. Fetal bovine serum (FBS) and culture medium were obtained from ExCell Bio (Shanghai, China). ^{14}C-labeled uric acid (55 mCi/mmol) was purchased from American Radiolabeled Chemicals, Inc. (St. Louis, MO). Lipofectamine 3000 kit was obtained from Invitrogen Canada, Inc. (Burlington, Ontario, Canada). PCR reagents like DNA polymerase and dNTPs were from Takara Bio, Inc. (Dalian, China). Goat anti-rabbit antibodies to hURAT1 (abs134382) and anti-Na^+-K^+-ATPase antibodies were purchased from Absin Bioscience, Inc. (Shanghai, China) and Santa Cruz Biotechnology (California), respectively. The plasma membrane isolation kit was obtained from Invent Biotechnologies, Inc. (Minnesota).

5.2. Plasmid Construction. Full-length cDNA (GenBank: AY639400.1) was inserted into the plasmid pcDNA3.1(+)-EGFP to express hURAT1. The cDNA of hURAT1 was PCR amplified using the DNA polymerase and the following primers: 5′-cttggtaccgagctcggatccgccaccatggca ttttctgaactcctgg-3′ (forward) and 5′-cttggtaccgagctcggatccgccaccatggcattttct-gaactcctgg-3′ (reverse). The resulting PCR product was digested with *Bam*HI and *Eco*RI enzymes and subsequently ligated to PcDNA3.1(+)-EGFP vector.

5.3. Cell Culture. HEK293T cells were purchased from ATCC and cultured in DMEM supplemented with 10% FBS at 37 °C in 5% CO_2. To facilitate cell adhesion, poly-D-lysine solution (0.1 mg/mL) was preincubated for 12 h in 24-well plates before plating the cells. When the cells reached around 80% confluence, 500 ng of plasmid was transferred into cells using lipofectamine 3000 reagent according to manufacturer's instructions.

5.4. ^{14}C-Uric Acid Uptake Assay. Twenty four hours after transfection, the culture medium was removed and the cells were incubated with uric acid uptake buffer containing 125 mM sodium gluconate, 4.8 mM potassium gluconate, 1.2 mM monobasic potassium phosphate, 1.2 mM magnesium sulfate, 1.3 mM calcium gluconate, and 5.6 mM glucose for 15 min. The uptake was initiated by adding 25 μM ^{14}C-uric acid for 20 min. The cells were washed three times with ice-cold DPBS to terminate the reaction. Cell lysates were obtained by adding 100 μL of 0.1 M sodium hydroxide. Intracellular radioactivity was determined using a liquid scintillation counter (PerkinElmer, Boston, MA) after adding 0.5 mL of scintillation fluid. The endogenous uptake in HEK293T mock cells was subtracted and corrected in WT and various hURAT1 mutants. Experiments were done in triplicate.

5.5. Western Blot. Twenty four hours after transfection in 60 mm dishes, the plasma membrane proteins were separated from HEK293T cells using plasma membrane isolation Kit (Invent, Minnesota) according to manufacturer's instructions. Plasma membrane proteins (20 μg) were loaded to 10% SDS-polyacrylamide gel, and electrophoresis was performed to resolve the proteins, followed by a transfer to the poly-(vinylidene fluoride) (PVDF) membranes. The membranes were blocked with 5% skim milk in TBS with 0.05% Tween 20 and incubated with either anti-URAT1 (1:1000) or anti-Na^+/K^+-ATPase (1:1000) antibodies at 4 °C overnight. Na^+/K^+-ATPase was used as the marker for plasma membrane proteins. After washing with PBS, the membranes were incubated with a goat anti-rabbit secondary antibody (Fdbio, Beijing, China) at room temperature for 1 h. The bands were developed with an ECL kit and visualized using a gel imaging system. The images were analyzed using ImageJ software (Maryland).

5.6. Site-Directed Mutagenesis. To obtain the mutants, forward and reverse oligonucleotides were prepared and used. The PcDNA3.1(+)-hURAT1-EGFP plasmid was prepared as the template by the PCR method. Briefly, primers of mutants were synthesized and added to the PCR cycling reaction to

https://dx.doi.org/10.1021/acsomega.0c05360
ACS Omega 2020, 5, 33421−33432

induce mutagenesis. Then, a restriction enzyme (*Dpn*I) was added to digest the nonmethylated template overnight. Digested PCR products were transformed into DMT competent cells (TransGen Biotech, Beijing, China) and cultured in solid Luria-Bertani plates with 1% ampicillin at 37 °C for 15 h. Single colibacillus colony was selected and amplified in Luria-Bertani liquid medium containing 1% NaCl, 1% tryptone, and 0.5% yeast extracts. All of the mutants were confirmed with automatic sequencing using ABI3730XL analyzer (Applied Biosystems, MA) to ensure the amino acid substitutions.

5.7. Uric Acid Kinetics Analysis. HEK293T cells transfected with hURAT1 or its mutants were incubated with the uric acid uptake buffer for 15 min. Then, different concentrations of ^{14}C-uric acid (10−200 μM) were added to initiate the uptake for 20 min. The endogenous uptake in HEK293T mock cells was subtracted and corrected in the kinetics studies for WT and various hURAT1 mutants. ^{14}C-uric acid uptake procedures were performed as described in Section 5.4. The K_m and V_{max} values were determined using Michaelis−Menten plots.

5.8. Constrained Consensus Prediction of Topology. To get an insight into the structural information of hURAT1, the protein sequence was downloaded from NCBI and submitted to the TOPDB database in fasta format. Topology localization of membrane spanning regions and orientation of segments are shown in Figure S1. The prediction presented in our work is a consensus of 10 different methods enhanced with available structural and experimental information from homologous proteins. CCTOP was tested on a benchmark set containing 170 proteins with known structures and achieved the highest accuracy among state-of-the-art and consensus methods.

5.9. Sequence Alignment and Homology Modeling. The protein sequence of hUART1 was retrieved from UniProt database (UniProt code: Q96S37) in fasta format. The results from Blast-p procedure of NCBI showed that the sequence identity was less than 30%. Different online tools like I-TASSER (http://zhanglab.ccmb.med.umich.edu/I-TASSER/) and Consurf were used to investigate the secondary structures, especially transmembrane regions and evolutionarily conserved residues, and to generate the models for comparison. Based on the topological characters of SLC22 family and functional similarity, the 3D structures including GLUTs and PiPT (PDB code: 5C65, 4J05, 4GBY, and 4GC0) were selected for multiple templates to generate 20 initial 3D models with MODELLER 9.13 software.[36] Top1 model with the best Z-DOPE score (a normalized atomic distance-dependent statistical potential based on known protein structures) was further optimized by Amber12. The final model was evaluated by SAVES (Structural Analysis and Verification Server) online server from UCLA (http://services.mbi.ucla.edu/SAVES/).

5.10. Induced Fit Docking Studies. Considering the flexibility of TMD7 and transport mechanisms of hURAT1, the docking experiments were done using the Schrödinger 2017 Induced Fit Docking (IFD) protocol,[57] in which side chain or backbone of the designated residue undergoes conformational changes to fit into the shape of active site and generate the closest conformer in the most reasonable binding mode. The protein structure was prepared and refined using the Protein Preparation Wizard of Schrödinger Maestro v11.1. Uric acid and small molecules were constructed by 2D sketcher, and their 3D structures were prepared using LigPrep to generate plausible ionization and tautomerization states at pH 7. The G361 residue was considered as the centroid of the binding site. IFD was carried out with the default parameters for the best hits using OPLS3[58] as the energy minimization force field. The initial docking positions within 30.0 kcal/mol of the top-ranking were re-docked using a Glide XP visualizer panel. The positions with highest-ranking Glide scores were reported to demonstrate the binding details.

5.11. Statistical Analysis. The differences between groups were assessed using analysis of variance (ANOVA) followed by Dunnett's test. The data were considered significant when the p value is <0.05. All of the statistical analyses were performed using GraphPad Prism 8.0 software (San Diego).

■ ASSOCIATED CONTENT

Supporting Information

The Supporting Information is available free of charge at https://pubs.acs.org/doi/10.1021/acsomega.0c05360.

Structure information of hURAT1 from 3D models (Table S1); conversed residue in TM7 and TM11 based on Consurf web server (Table S2); sequence similarity of hURAT1 to selected proteins based on I-TASSER (Table S3); results of transmembrane regions of hURAT1 predicted by CCTOP web server (Figure S1); and Ramachandran plot of hURAT1 outward model (Figure S2) (PDF)

■ AUTHOR INFORMATION

Corresponding Authors

Yuanxin Tian − *School of Pharmaceutical Sciences, Southern Medical University, Guangzhou, Guangdong 510515, China*; orcid.org/0000-0003-3847-559X; Email: tyx523@163.com

Jianxin Pang − *School of Pharmaceutical Sciences, Southern Medical University, Guangzhou, Guangdong 510515, China*; orcid.org/0000-0002-0053-2723; Phone: +86(20)61648671; Email: pjx@smu.edu.cn; Fax: +86(20)61648671

Authors

Ze'an Zhao − *School of Pharmaceutical Sciences, Southern Medical University, Guangzhou, Guangdong 510515, China*

Yu Jiang − *School of Pharmaceutical Sciences, Southern Medical University, Guangzhou, Guangdong 510515, China*

Lu Li − *School of Pharmaceutical Sciences, Southern Medical University, Guangzhou, Guangdong 510515, China*

Yanyu Chen − *School of Pharmaceutical Sciences, Southern Medical University, Guangzhou, Guangdong 510515, China*

Yongmei Li − *School of Pharmaceutical Sciences, Southern Medical University, Guangzhou, Guangdong 510515, China*

Qunsheng Lan − *School of Pharmaceutical Sciences, Southern Medical University, Guangzhou, Guangdong 510515, China*

Ting Wu − *School of Pharmaceutical Sciences, Southern Medical University, Guangzhou, Guangdong 510515, China*

Cuiting Lin − *School of Pharmaceutical Sciences, Southern Medical University, Guangzhou, Guangdong 510515, China*

Ying Cao − *School of Pharmaceutical Sciences, Southern Medical University, Guangzhou, Guangdong 510515, China*

Kutty Selva Nandakumar − *School of Pharmaceutical Sciences, Southern Medical University, Guangzhou, Guangdong 510515, China*; orcid.org/0000-0001-7790-8197

https://dx.doi.org/10.1021/acsomega.0c05360
ACS Omega 2020, 5, 33421−33432

Pingzheng Zhou − *School of Pharmaceutical Sciences, Southern Medical University, Guangzhou, Guangdong 510515, China*

Complete contact information is available at: https://pubs.acs.org/10.1021/acsomega.0c05360

Author Contributions

Q.L., Y.C., and Y.L. participated in research design. P.Z., J.P., and Y.T. conducted experiments. C.L. contributed new reagents or analytic tools. Y.J. and Y.C. performed data analysis. Z.Z., L.L., T.W., and K.S.N. wrote or contributed to the writing of the manuscript.

Notes

The authors declare no competing financial interest.

■ ACKNOWLEDGMENTS

The authors thank professor Banghao Zhu and Guangyun Lin from Sun Yat-sen University for their help in ^{14}C-uric acid uptake assays. This research was funded by the Natural Science Foundation of China (grant numbers 81773794 and 81974507) and Natural Science Foundation of Guangdong Province (grant number 2018A0303130088).

■ REFERENCES

(1) Nigam, S. K.; Bush, K. T.; Martovetsky, G.; Ahn, S. Y.; Liu, H. C.; Richard, E.; Bhatnagar, V.; Wu, W. The organic anion transporter (OAT) family: a systems biology perspective. *Physiol. Rev.* **2015**, *95*, 83−123.

(2) Rizwan, A. N.; Burckhardt, G. Organic anion transporters of the SLC22 family: biopharmaceutical, physiological, and pathological roles. *Pharm. Res.* **2007**, *24*, 450−470.

(3) Nigam, S. K.; Bush, K. T.; Martovetsky, G.; Ahn, S. Y.; Liu, H. C.; Richard, E.; Bhatnagar, V.; Wu, W. The organic anion transporter (OAT) family: a systems biology perspective. *Physiol. Rev.* **2015**, *95*, 83−123.

(4) Tin, A.; Li, Y.; Brody, J. A.; Nutile, T.; Chu, A. Y.; Huffman, J. E.; Yang, Q.; Chen, M. H.; Robinson-Cohen, C.; Mace, A.; et al. Large-scale whole-exome sequencing association studies identify rare functional variants influencing serum urate levels. *Nat. Commun.* **2018**, *9*, No. 4228.

(5) Nakanishi, T.; Ohya, K.; Shimada, S.; Anzai, N.; Tamai, I. Functional cooperation of URAT1 (SLC22A12) and URATv1 (SLC2A9) in renal reabsorption of urate. *Nephrol., Dial., Transplant.* **2013**, *28*, 603−611.

(6) Köttgen, A.; Albrecht, E.; Teumer, A.; Vitart, V.; Krumsiek, J.; Hundertmark, C.; Pistis, G.; Ruggiero, D.; O'Seaghdha, C. M.; Haller, T.; et al. Genome-wide association analyses identify 18 new loci associated with serum urate concentrations. *Nat. Genet.* **2013**, *45*, 145−154.

(7) Enomoto, A.; Kimura, H.; Chairoungdua, A.; Shigeta, Y.; Jutabha, P.; Cha, S. H.; Hosoyamada, M.; Takeda, M.; Sekine, T.; Igarashi, T.; et al. Molecular identification of a renal urate anion exchanger that regulates blood urate levels. *Nature* **2002**, *417*, 447−452.

(8) Becker, M. A.; Schumacher, H. J.; Wortmann, R. L.; MacDonald, P. A.; Eustace, D.; Palo, W. A.; Streit, J.; Joseph-Ridge, N. Febuxostat compared with allopurinol in patients with hyperuricemia and gout. *N. Engl. J. Med.* **2005**, *353*, 2450−2461.

(9) Yan, N. Structural Biology of the Major Facilitator Superfamily Transporters. *Annu. Rev. Biophys.* **2015**, *44*, 257−283.

(10) Reddy, V. S.; Shlykov, M. A.; Castillo, R.; Sun, E. I.; Saier, M. J. The major facilitator superfamily (MFS) revisited. *FEBS J.* **2012**, *279*, 2022−2035.

(11) Law, C. J.; Maloney, P. C.; Wang, D. N. Ins and outs of major facilitator superfamily antiporters. *Annu. Rev. Microbiol.* **2008**, *62*, 289−305.

(12) Quistgaard, E. M.; Low, C.; Guettou, F.; Nordlund, P. Understanding transport by the major facilitator superfamily (MFS): structures pave the way. *Nat. Rev. Mol. Cell Biol.* **2016**, *17*, 123−132.

(13) Popp, C.; Gorboulev, V.; Muller, T. D.; Gorbunov, D.; Shatskaya, N.; Koepsell, H. Amino acids critical for substrate affinity of rat organic cation transporter 1 line the substrate binding region in a model derived from the tertiary structure of lactose permease. *Mol. Pharmacol.* **2005**, *67*, 1600−1611.

(14) Egenberger, B.; Gorboulev, V.; Keller, T.; Gorbunov, D.; Gottlieb, N.; Geiger, D.; Mueller, T. D.; Koepsell, H. A substrate binding hinge domain is critical for transport-related structural changes of organic cation transporter 1. *J. Biol. Chem.* **2012**, *287*, 31561−31573.

(15) Keller, T.; Egenberger, B.; Gorboulev, V.; Bernhard, F.; Uzelac, Z.; Gorbunov, D.; Wirth, C.; Koppatz, S.; Dotsch, V.; Hunte, C.; et al. The large extracellular loop of organic cation transporter 1 influences substrate affinity and is pivotal for oligomerization. *J. Biol. Chem.* **2011**, *286*, 37874−37886.

(16) Li, D. C.; Nichols, C. G.; Sala-Rabanal, M. Role of a Hydrophobic Pocket in Polyamine Interactions with the Polyspecific Organic Cation Transporter OCT3. *J. Biol. Chem.* **2015**, *290*, 27633−27643.

(17) Roth, M.; Obaidat, A.; Hagenbuch, B. OATPs, OATs and OCTs: the organic anion and cation transporters of the SLCO and SLC22A gene superfamilies. *Br. J. Pharmacol.* **2012**, *165*, 1260−1287.

(18) Holyoake, J.; Sansom, M. S. Conformational change in an MFS protein: MD simulations of LacY. *Structure* **2007**, *15*, 873−884.

(19) Smirnova, I.; Kasho, V.; Choe, J. Y.; Altenbach, C.; Hubbell, W. L.; Kaback, H. R. Sugar binding induces an outward facing conformation of LacY. *Proc. Natl. Acad. Sci. U.S.A.* **2007**, *104*, 16504−16509.

(20) Madej, M. G.; Soro, S. N.; Kaback, H. R. Apo-intermediate in the transport cycle of lactose permease (LacY). *Proc. Natl. Acad. Sci. U.S.A.* **2012**, *109*, E2970−E2978.

(21) Eraly, S. A.; Hamilton, B. A.; Nigam, S. K. Organic anion and cation transporters occur in pairs of similar and similarly expressed genes. *Biochem. Biophys. Res. Commun.* **2003**, *300*, 333−342.

(22) Hong, M.; Li, S.; Zhou, F.; Thomas, P. E.; You, G. Putative transmembrane domain 12 of the human organic anion transporter hOAT1 determines transporter stability and maturation efficiency. *J. Pharmacol. Exp. Ther.* **2010**, *332*, 650−658.

(23) Xu, W.; Tanaka, K.; Sun, A. Q.; You, G. Functional role of the C terminus of human organic anion transporter hOAT1. *J. Biol. Chem.* **2006**, *281*, 31178−31183.

(24) Perry, J. L.; Dembla-Rajpal, N.; Hall, L. A.; Pritchard, J. B. A three-dimensional model of human organic anion transporter 1: aromatic amino acids required for substrate transport. *J. Biol. Chem.* **2006**, *281*, 38071−38079.

(25) Zhou, F.; Zhu, L.; Cui, P. H.; Church, W. B.; Murray, M. Functional characterization of nonsynonymous single nucleotide polymorphisms in the human organic anion transporter 4 (hOAT4). *Br. J. Pharmacol.* **2010**, *159*, 419−427.

(26) Feng, B.; Dresser, M. J.; Shu, Y.; Johns, S. J.; Giacomini, K. M. Arginine 454 and lysine 370 are essential for the anion specificity of the organic anion transporter, rOAT3. *Biochemistry* **2001**, *40*, 5511−5520.

(27) Tanaka, K.; Zhou, F.; Kuze, K.; You, G. Cysteine residues in the organic anion transporter mOAT1. *Biochem. J.* **2004**, *380*, 283−287.

(28) Chu, X. Y.; Bleasby, K.; Yabut, J.; Cai, X.; Chan, G. H.; Hafey, M. J.; Xu, S.; Bergman, A. J.; Braun, M. P.; Dean, D. C.; et al. Transport of the dipeptidyl peptidase-4 inhibitor sitagliptin by human organic anion transporter 3, organic anion transporting polypeptide 4C1, and multidrug resistance P-glycoprotein. *J. Pharmacol. Exp. Ther.* **2007**, *321*, 673−683.

(29) Gorboulev, V.; Shatskaya, N.; Volk, C.; Koepsell, H. Subtype-specific affinity for corticosterone of rat organic cation transporters rOCT1 and rOCT2 depends on three amino acids within the substrate binding region. *Mol. Pharmacol.* **2005**, *67*, 1612−1619.

(30) Tan, P. K.; Liu, S.; Gunic, E.; Miner, J. N. Discovery and characterization of verinurad, a potent and specific inhibitor of URAT1 for the treatment of hyperuricemia and gout. *Sci. Rep.* **2017**, *7*, No. 665.
(31) Dobson, L.; Remenyi, I.; Tusnady, G. E. CCTOP: a Consensus Constrained TOPology prediction web server. *Nucleic Acids Res.* **2015**, *43*, W408−W412.
(32) Tan, P. K.; Ostertag, T. M.; Miner, J. N. Mechanism of high affinity inhibition of the human urate transporter URAT1. *Sci. Rep.* **2016**, *6*, No. 34995.
(33) Gorboulev, V.; Volk, C.; Arndt, P.; Akhoundova, A.; Koepsell, H. Selectivity of the polyspecific cation transporter rOCT1 is changed by mutation of aspartate 475 to glutamate. *Mol. Pharmacol.* **1999**, *56*, 1254−1261.
(34) Gorbunov, D.; Gorboulev, V.; Shatskaya, N.; Mueller, T.; Bamberg, E.; Friedrich, T.; Koepsell, H. High-affinity cation binding to organic cation transporter 1 induces movement of helix 11 and blocks transport after mutations in a modeled interaction domain between two helices. *Mol. Pharmacol.* **2008**, *73*, 50−61.
(35) Yang, J.; Zhang, Y. I-TASSER server: new development for protein structure and function predictions. *Nucleic Acids Res.* **2015**, *43*, W174−W181.
(36) Fiser, A.; Do, R. K.; Sali, A. Modeling of loops in protein structures. *Protein Sci.* **2000**, *9*, 1753−1773.
(37) Garibsingh, R. A.; Otte, N. J.; Ndaru, E.; Colas, C.; Grewer, C.; Holst, J.; Schlessinger, A. Homology Modeling Informs Ligand Discovery for the Glutamine Transporter ASCT2. *Front. Chem.* **2018**, *6*, No. 279.
(38) van Aalten, D. M.; Bywater, R.; Findlay, J. B.; Hendlich, M.; Hooft, R. W.; Vriend, G. PRODRG, a program for generating molecular topologies and unique molecular descriptors from coordinates of small molecules. *J. Comput.-Aided Mol. Des.* **1996**, *10*, 255−262.
(39) Pedersen, B. P.; Kumar, H.; Waight, A. B.; Risenmay, A. J.; Roe-Zurz, Z.; Chau, B. H.; Schlessinger, A.; Bonomi, M.; Harries, W.; Sali, A.; et al. Crystal structure of a eukaryotic phosphate transporter. *Nature* **2013**, *496*, 533−536.
(40) Enomoto, A.; Kimura, H.; Chairoungdua, A.; Shigeta, Y.; Jutabha, P.; Cha, S. H.; Hosoyamada, M.; Takeda, M.; Sekine, T.; Igarashi, T.; et al. Molecular identification of a renal urate anion exchanger that regulates blood urate levels. *Nature* **2002**, *417*, 447−452.
(41) Dong, Y.; Zhao, T.; Ai, W.; Zalloum, W. A.; Kang, D.; Wu, T.; Liu, X.; Zhan, P. Novel urate transporter 1 (URAT1) inhibitors: a review of recent patent literature (2016-2019). *Expert Opin. Ther. Pat.* **2019**, *29*, 871−879.
(42) Koepsell, H. The SLC22 family with transporters of organic cations, anions and zwitterions. *Mol. Aspects Med.* **2013**, *34*, 413−435.
(43) Koepsell, H.; Endou, H. The SLC22 drug transporter family. *Pfluegers Arch.* **2004**, *447*, 666−676.
(44) Forrest, L. R.; Kramer, R.; Ziegler, C. The structural basis of secondary active transport mechanisms. *Biochim. Biophys. Acta* **2011**, *1807*, 167−188.
(45) Solcan, N.; Kwok, J.; Fowler, P. W.; Cameron, A. D.; Drew, D.; Iwata, S.; Newstead, S. Alternating access mechanism in the POT family of oligopeptide transporters. *EMBO J.* **2012**, *31*, 3411−3421.
(46) Pace, C. N.; Scholtz, J. M. A helix propensity scale based on experimental studies of peptides and proteins. *Biophys. J.* **1998**, *75*, 422−427.
(47) Egenberger, B.; Gorboulev, V.; Keller, T.; Gorbunov, D.; Gottlieb, N.; Geiger, D.; Mueller, T. D.; Koepsell, H. A substrate binding hinge domain is critical for transport-related structural changes of organic cation transporter 1. *J. Biol. Chem.* **2012**, *287*, 31561−31573.
(48) Iancu, C. V.; Zamoon, J.; Woo, S. B.; Aleshin, A.; Choe, J. Y. Crystal structure of a glucose/H+ symporter and its mechanism of action. *Proc. Natl. Acad. Sci. U.S.A.* **2013**, *110*, 17862−17867.
(49) Jiang, D.; Zhao, Y.; Wang, X.; Fan, J.; Heng, J.; Liu, X.; Feng, W.; Kang, X.; Huang, B.; Liu, J.; et al. Structure of the YajR transporter suggests a transport mechanism based on the conserved motif A. *Proc. Natl. Acad. Sci. U.S.A.* **2013**, *110*, 14664−14669.
(50) Dang, S.; Sun, L.; Huang, Y.; Lu, F.; Liu, Y.; Gong, H.; Wang, J.; Yan, N. Structure of a fucose transporter in an outward-open conformation. *Nature* **2010**, *467*, 734−738.
(51) Kumar, H.; Kasho, V.; Smirnova, I.; Finer-Moore, J. S.; Kaback, H. R.; Stroud, R. M. Structure of sugar-bound LacY. *Proc. Natl. Acad. Sci. U.S.A.* **2014**, *111*, 1784−1788.
(52) Deng, D.; Sun, P.; Yan, C.; Ke, M.; Jiang, X.; Xiong, L.; Ren, W.; Hirata, K.; Yamamoto, M.; Fan, S.; et al. Molecular basis of ligand recognition and transport by glucose transporters. *Nature* **2015**, *526*, 391−396.
(53) Dang, S.; Sun, L.; Huang, Y.; Lu, F.; Liu, Y.; Gong, H.; Wang, J.; Yan, N. Structure of a fucose transporter in an outward-open conformation. *Nature* **2010**, *467*, 734−738.
(54) Sun, L.; Zeng, X.; Yan, C.; Sun, X.; Gong, X.; Rao, Y.; Yan, N. Crystal structure of a bacterial homologue of glucose transporters GLUT1-4. *Nature* **2012**, *490*, 361−366.
(55) Rizwan, A. N.; Krick, W.; Burckhardt, G. The chloride dependence of the human organic anion transporter 1 (hOAT1) is blunted by mutation of a single amino acid. *J. Biol. Chem.* **2007**, *282*, 13402−13409.
(56) Zhao, T.; Meng, Q.; Sun, Z.; Chen, Y.; Ai, W.; Zhao, Z.; Kang, D.; Dong, Y.; Liang, R.; Wu, T.; et al. Novel Human Urate Transporter 1 Inhibitors as Hypouricemic Drug Candidates with Favorable Druggability. *J. Med. Chem.* **2020**, *63*, 10829−10854.
(57) Li, G.; Li, W.; Xie, Y.; Wan, X.; Zheng, G.; Huang, N.; Zhou, Y. Discovery of Novel Pim-1 Kinase Inhibitors with a Flexible-Receptor Docking Protocol. *J. Chem. Inf. Model.* **2019**, *59*, 4116−4119.
(58) Harder, E.; Damm, W.; Maple, J.; Wu, C.; Reboul, M.; Xiang, J. Y.; Wang, L.; Lupyan, D.; Dahlgren, M. K.; Knight, J. L.; et al. OPLS3: A Force Field Providing Broad Coverage of Drug-like Small Molecules and Proteins. *J. Chem. Theory Comput.* **2016**, *12*, 281−296.

https://dx.doi.org/10.1021/acsomega.0c05360
ACS Omega 2020, 5, 33421−33432